Ice-templated additive-free porous starches with tuned morphology and properties

Fangxin Zou, Jean-Luc Bouvard, Christophe Pradille, Tatiana Budtova

Ice-templated Additive-free Porous Starches with Tuned Morphology and Properties

Fangxin Zou[a], Jean-Luc Bouvard[a], Christophe Pradille[b], Tatiana Budtova[a]*

[a] MINES Paris, PSL Research University, Center for Materials Forming (CEMEF), UMR CNRS 7635, CS 10207, 06904 Sophia Antipolis, France

[b] Mat Xper, 19 Traverse du Barri, 06560, Sophia Antipolis, France

* Corresponding author: Tatiana Budtova, e-mail address: tatiana.budtova@minesparis.psl.eu

Abstract

Biodegradable anisotropic neat porous starch materials without any additional cross-linking, plasticizer or any extra matter have been fabricated via facile ice-templating method. Waxy maize was dissolved in water followed by unidirectional freezing and ice sublimation. The influence of process parameters (starch concentration and retrogradation time) on the morphology, density, mechanical properties under the uniaxial compression and thermal conductivity were investigated. The internal morphology and the shape of the pores, from lamellar to sponge-like, was shown to be governed by starch concentration. All porous starches have very low density (0.07-0.15 g/cm^3), anisotropic mechanical properties and low thermal conductivity, in particular in transverse direction (0.037-0.048 W/(m·K)). Interestingly, when compressing the ice-templated starches in the transverse direction, the thermal conductivity was further decreased reaching the values of 0.033 W/(m·K). This work provides the guidelines for making fully biobased porous starch materials with controlled morphology and properties.

Keywords: waxy maize starch, unidirectional freezing, lyophilization, anisotropy, density, mechanical properties, thermal conductivity

1. Introduction

Polymer cellular materials are widely used in numerous applications as materials for packaging, thermal or acoustic insulation, shock absorbers, bio-medical scaffolds, etc. With the goal to reduce the environmental impact of synthetic polymer industry and to realize a sustainable society, bio-based polymer foams and aerogels attract more and more attention [1]. Starch is one of the most abundant, widely available, biodegradable and inexpensive polysaccharides; its foams of various morphology and properties can be made via extrusion or baking starch pastes at high temperature, microwave heating, freeze-drying or drying under supercritical conditions [2–4]. Freeze-drying of starches is used for various applications: for the preservation of granules, for modification of starch digestion, for encapsulation and release of active compounds and for making biomimetic templates [5–7]. Thermal conductivity of porous starch-based materials has also been considered recently in the view of applications for thermal insulation [8,9].

Freeze-drying is widely applied in industry to make porous materials or powders. It consists of freezing the solvent in a system followed by the sublimation of solvent crystals (often ice in case of aqueous solutions). The resulting material is light-weight, with open porosity and interconnected macropores. Freeze-drying also allows the fabrication of porous materials with anisotropic morphology by varying and controlling crystals' growth direction using, for example, unidirectional freezing and removing the solvent by sublimation (or lyophilization); it is also called ice-templating or freeze-casting [10]. This can be of a particular interest for biological, tissue engineering and biotechnological applications if the solid phase is based on a biocompatible matter [11].

To obtain starch-based porous materials, freeze-drying has been applied on various starches in different initial states: granules [5], solutions [7,12], emulsions [13] and gels from retrograded

starch [4,14–16]. As the majority of starches contain amylose which is retrograding quickly, freeze-dried starches are made from gels [4,14–16]. Often starches are plasticized [12] and/or mixed with other matters [7,17,18]. Only few articles report on porous materials made from starches that are based on amylopectin [7,17]: as amylopectin retrogradation is slow and thus freeze-drying is performed from solutions, reinforcing fibers such as microfibrillated cellulose [7] or nanochitin [17] have been used.

Few words have to be said about the terminology found in literature to name some porous materials "cryogels" and "aerogels". Strictly speaking, "cryogels" are materials in which freezing induces gelation [19]. If no gelation occurs upon freezing and a porous material is formed after freezing and lyophilisation, it is called a "cryostructurate"; without any post-treatment it is soluble in the solvent which was removed by lyophilization [19]. Cryostructurate is also a material based on a gel in which the solvent is frozen and removed [19]. "Aerogels" are materials with low density and high specific surface area [20]. IUPAC gives the definition of an aerogel as "a gel comprised of a microporous solid in which the dispersed phase is a gas" [21]; however, this definition is too restrictive as it excludes even classical mesoporous silica aerogels. Aerogels scientists agree that aerogels are dry open pores nanostructured (mesoporous with small macropores) materials with high porosity (above 90%) and high specific surface area (at least above 100 m^2/g) [1,22].

In our previous work we demonstrated that amylose/amylopectin ratio, and thus the initial state of dissolved starch (gel vs solution) before freeze-drying, significantly influence the morphology and properties of the dry material [15]. Retrograded starch with higher amylose content formed stronger gels which were better "resisting" to the growth of ice crystals. For example, the pores in the retrograded and freeze-dried pea starch (33 – 36% amylose) did not show any preferential pore orientation under unidirectional freezing and ice sublimation; at the same concentration potato

starch (18 – 21 % amylose) gels are weaker than those of pea starch and pores became slightly oriented. Freeze-drying of the weakest gels based on retrograded (30-45 days) waxy maize starch possessed strongly oriented pores in the direction of the growth of ice crystals. It was thus concluded that waxy maize starch is suitable for ice templating but no further study of the properties of these materials was performed.

The goal of this work is to make ice-templated starches with no additional cross-linking, no plasticizer and no additional matter; we hypothesize that such neat porous starch materials (or cryostructurates) can possess properties that compete with freeze-dried starches containing various additives (either plasticizers and/or reinforcing agents). The starch was waxy maize (amylopectin) and the solvent was water; unidirectional freezing followed by ice sublimation was used. The influence of starch concentration and retrogradation time as well as pores' orientation on the final material morphology and properties (density, specific surface area, mechanical properties under the uniaxial compression and thermal conductivity) were systematically studied.

2. Experimental Section

2.1 Materials

Waxy maize starch N-200 with amylose content around 1% was kindly provided by Roquette, France, and used without any further purification. Distillated water was used.

2.2 Preparation of waxy maize porous starch materials by ice-templating method

Waxy maize porous starches were prepared through the following steps: dissolution-retrogradation-ice templating (Fig. 1). Waxy maize starch solutions of 5, 8 and 11 wt% (in dry weight) were prepared using our previous method [15]: starch was mixed with distilled water at room temperature for 5 min, then heated up to 95 °C under stirring at 1000 rpm, and stirred for

another 3 h. In these conditions waxy maize starch is dissolved with no granule remnants (Fig. S1). Hot starch solutions were centrifuged for 3 min under 8000 rpm to remove air bubbles. After cooling down to room temperature, solutions were placed in cubic moulds (30 mm edge) made of Teflon™ with a metal plate at the bottom and stored at 4 °C for retrogradation during 3, 7 and 11 days. No gelation within this retrogradation time was recorded [15].

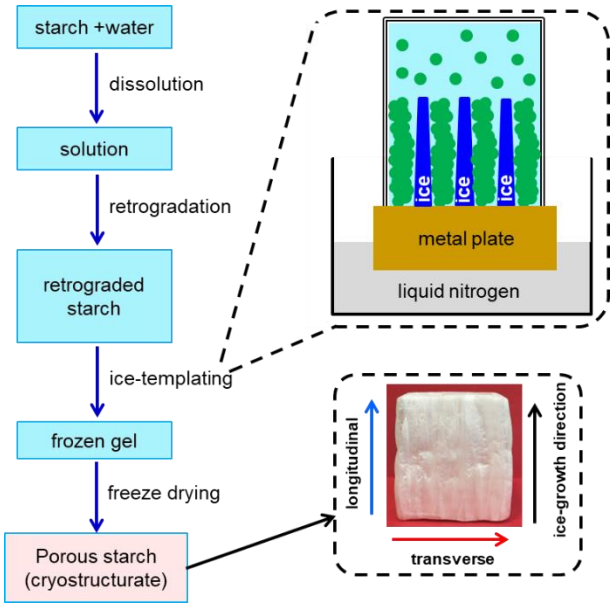

Fig. 1.

Schematic illustration of the processing route for making anisotropic waxy maize porous starches (or cryostructurates).

The ice-templating process was performed by placing the metal plate of the mould in the liquid nitrogen and keeping until starch solution is frozen (see Fig. 1). Water from the frozen sample was sublimated for 4 days by using the Lyophilisateur Cryotec COSMOS-80 (Cryotec) at - 82 °C and pressure below 2 mTorr. In the following, the waxy maize porous starches are named as "X wt%-N days", where X is the starch concentration in solution and N is retrogradation time. The "transverse" and "longitudinal" directions will be used in the following to indicate the direction

perpendicular and parallel to the ice crystals' growth, respectively, as illustrated in Fig. 1. We name the final material obtained after lyophilization a "porous starch" or a "cryostructurate" as it can be dissolved in the conditions used for the dissolution of the initial waxy maize starch.

2.3 Characterization

2.3.1 Bulk density and porosity

Bulk density ρ_{bulk} of waxy maize porous starches calculated from the measurements of sample volume made with a digital caliper and weight with high-precision digital balance. The porosity and pores' specific volume were calculated from bulk and skeletal density $\rho_{skeletal}$ (the latter taken as 1.45 g/cm^3) [23].

$$porosity\ (\%) = \left(1 - \frac{\rho_{bulk}}{\rho_{skeletal}}\right) \times 100\% \quad (1)$$

$$pore\ volume = \frac{1}{\rho_{bulk}} - \frac{1}{\rho_{skeletal}} \quad (2)$$

2.3.2 Specific surface area

Specific surface area of waxy maize porous starch was determined using the Brunauer, Emmett and Teller (BET) method with ASAP 2020 specific surface area and porosity analyzer (Micromeritics Instrument Corporation). Prior to the measurement, all samples were degassed at 70 °C for 10 h.

2.3.3 Morphology

The morphology (internal cross-section) was characterized by Scanning Electron Microscope (SEM) MAIA 3 (TESCAN) with an accelerating voltage of 3 kV. Before the measurements, a roughly 14 nm thin layer of platinum was sputtered onto the sample's surface with Q150T coater (Quorum). Pore density was calculated by analysing SEM images of the cross-sections of samples using ImageJ software as follows: i) for 5 wt% samples from the number of slit pores within 1 mm

(at least 200 individual pores were analyzed); ii) for 8 wt% and 11 wt% samples from the number of honeycomb or spherical pores within 1 mm^2 area (at least 8 SEM images with magnification × 2000 were anaysed). Pore wall thickness was also estimated from SEM images using ImageJ software (at least 100 pore walls analyzed).

2.3.4 Mechanical properties under compression

Mechanical properties of waxy maize porous starches under the uniaxial compression were analyzed using Instron 5967 testing machine equipped with a 30 kN load cell. This load cell has been calibrated in class 0.5 (i. e 0.5% of error, per ISO 376:2011) in the range of 1/300 and 100% of the nominal load. The error is lower than 1% of the nominal load in the range from 2 N to 100 N. All samples were cut into cubes with around 1 cm^3 edge with using a razor blade, the planes were checked to be parallel and planar. The compression rate was 1 mm/min. A preload of 1 N was used to ensure the contact with the sample. Compressive modulus was calculated from the initial linear region (up to ≈ 3% strain) of nominal stress-strain dependence. For higher strains, stress at 40% strain and compression toughness (or energy absorbed) up to 40% strain were also calculated.

2.3.5 Thermal conductivity

Thermal conductivity was measured using steady-state method with a standard Fox150 Thermal Conductivity Meter (Laser Comp) equipped with a custom micro-flow meter developed for small samples [24,25]. The samples were square plates of about 30 mm in side and 28 mm in thickness. The sample was placed between two plates; one of them is heated, the temperature of the other plate was recorded and thermal conductivity calculated from temperature difference. The calibration was carried out with i) a fibrous-glass board reference material IRMM 440-A, NIST 1450b SRM, thermal conductivity at 23°C 0.03194 W/(m·K) and ii) a superinsulating commercial

material of thermal conductivity at 23°C 0.016 W/(m·K), obtained according to a standard NF EN 12667.

3. Results and discussion

3.1 Density, porosity, pore volume and morphology of waxy maize porous starch materials

Density is the main parameter characterizing a porous material; it is shown in Fig. 2a for waxy maize porous starches for three starch concentrations in the initial solution as a function of retrogradation time. All densities are very low, and increase with the increase of starch concentration, as expected. No influence of retrogradation time was recorded, within the experimental errors. The porosity of the obtained materials is presented in Fig. S2; it varies from 90 to 95% for starch concentrations from 11 to 5 wt%, respectively. Pore volume is high, from about 5 to 14 cm^3/g (Fig. 2b). It is comparable with pore volume in cellulose II aerogels (10 – 25 cm^3/g) [26] or pectin aerogels (10 – 30 cm^3/g) [24].

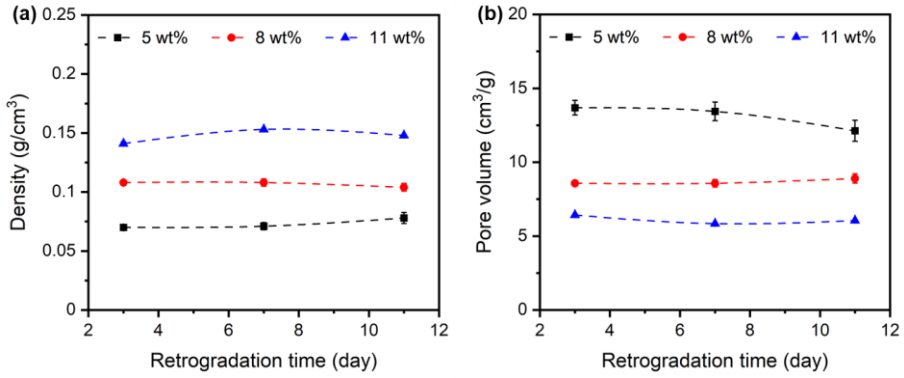

Fig. 2.

Density (a) and pore volume (b) of waxy maize porous starches from different starch concentrations as a function of retrogradation time. If the errors are not seen, they are smaller or equal to the symbol. Lines are given to guide the eye.

The representative images of the morphology of waxy maize porous starches are demonstrated in Fig. 3; they show the cross-sections perpendicular to the ice-growth direction. Similar morphology was observed for other retrogradation times (see Fig. S3 of the Supporting Information). The increase in starch concentration leads to a significant modification of pore structure (Fig. 3a): from big slit pores at 5 wt% concentration to medium irregular honeycomb-like pores at 8 wt% followed by smaller spherical pores at 11 wt%. Because of the significant change of pore shape for samples from low (5 wt%) to higher (8 and 11 wt%) starch concentration, it was not possible to evaluate the influence of starch concentration on pores' dimensions. Thus, pore density was roughly estimated (see Methods section); it is presented in Fig. S4. As expected, pore density increases with the increase of starch concentration.

As the freezing conditions are the same in all cases, the morphology is controlled by starch concentration. The growing ice crystals induce a significant increase in starch concentration within the volume of the so-called "unfrozen liquid microphase" [19]. At low starch concentration, the lamellar structure is formed with the walls connected by "bridges" that not always "reach" the opposite lamella (Fig. 3a). With the increase of starch concentration more and more bridges are formed between lamellas (Fig. 3b). Further increase of starch concentration leads to a formation of a "spongy" matrix without any distinction between lamellas and bridges (Fig. 3c). These types of pores' structures have been reported for other organic or inorganic ice-templated porous materials [10], but, to the best of our knowledge, not for any neat non-crosslinked polysaccharide cryogenic structure made from the same precursor. Retrogradation time does not significantly change either pore type or dimensions within the same starch concentration. Pore wall thickness, roughly estimated by image analysis, varies from 0.4 to 0.8 μm and does not depend on starch concentration or retrogradation time.

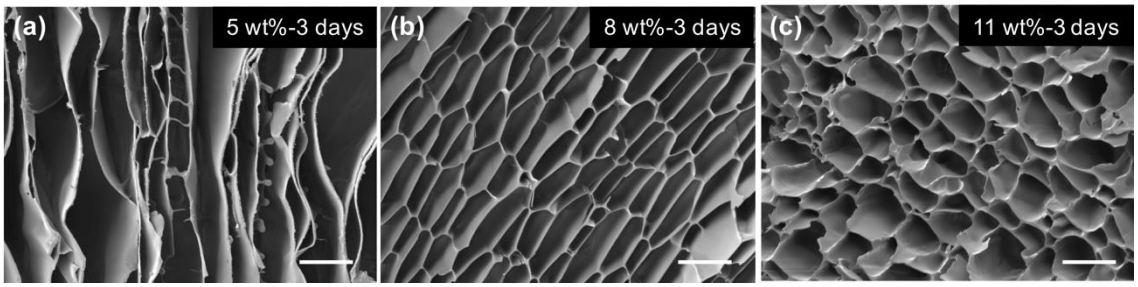

Fig. 3.

SEM images of the cross-section of waxy maize porous starches made from starch concentrations of 5 wt% (a), 8 wt% (b) and 11 wt% (c), all after 3 days retrogradation. Scale bars are 20 μm.

The specific surface area of all obtained materials is very low, within 3 - 5 m^2/g, and does not depend either on starch concentration or retrogradation time. These low values correlate with very large macropores, as seen in Fig. 3 and Fig. S3, and reflect the absence of mesoporosity. Similar low values were obtained for freeze-dried retrograded potato starch [15,16] and amylomaize starch (67% amylose) [16].

3.2 Mechanical properties

The mechanical properties of waxy maize porous starch materials were tested under the uniaxial compression in the directions parallel (longitudinal) and perpendicular (transversal) to the growth of ice crystals (Fig. 4a). The examples of stress-strain curves are shown in Fig. 4b. No breakage was observed within the interval of strains applied. The curves exhibit three regions, in particular well defined for the compression in the longitudinal direction, and typical for porous materials: an elastic region up to few strains per cent, a plastic deformation plateau and a final densification region.

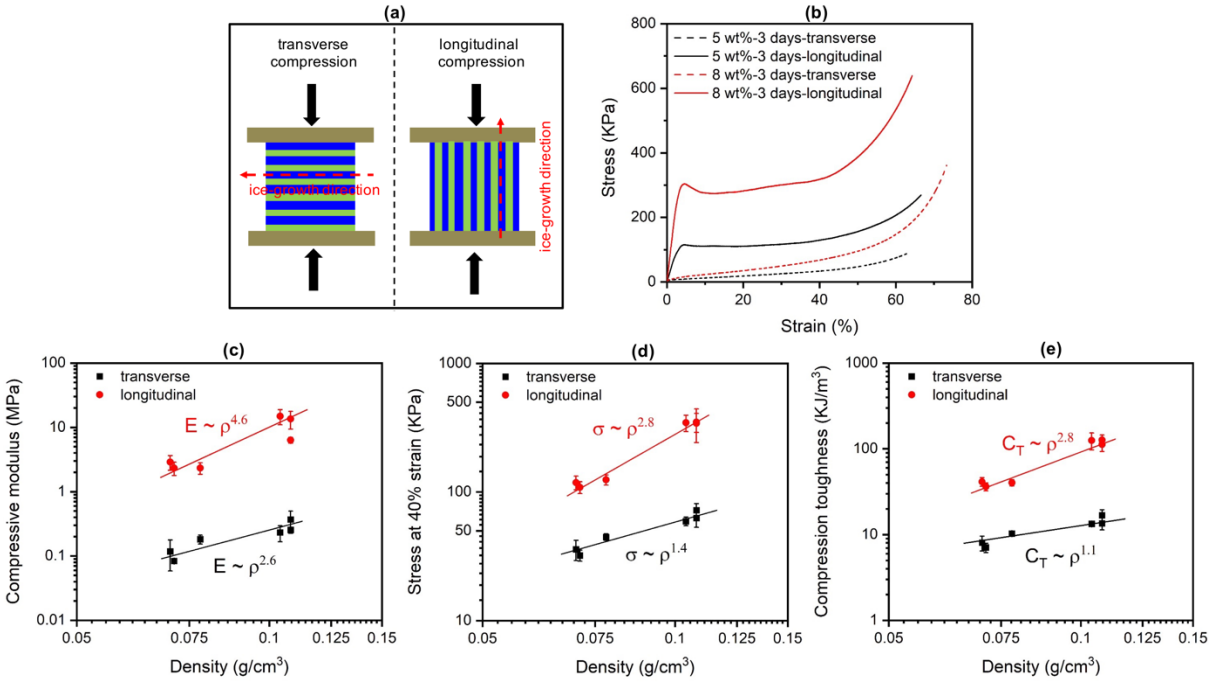

Fig. 4.

Schematic illustration of the uniaxial compression of porous starches in two different directions (a), representative stress-strain curves for 5 wt%-3 days and 8 wt%-3 days materials (b), compressive modulus (c), stress at 40% strain (d) and compression toughness (d) as a function of material bulk density.

The stresses in the longitudinal direction are much higher than in the transverse direction, as expected, and as reported for other anisotropic porous materials, bio-based [27–31] or not [32,33], with similar shapes of stress-strain curves [27,33]. All characteristics are plotted as a function of material density (Fig. 4c-e). Compressive modulus, stress at 40% strain and toughness in the longitudinal direction are several times higher than those in the transverse direction which correlates well with trends reported for anisotropic foams [32]. All characteristics increase with porous starch density (Fig. 4c-e), as expected. They were approximated by power-law dependences, as predicted for foams [32] and also aerogels [34,35]. The scaling exponent for compressive

modulus is around 2.6 ± 0.56 for the transverse direction and 4.6 ± 1.39 for the longitudinal direction. These values are higher than the one predicted for classical open-cell foams (modulus proportional to foams density in power 2) [32] and similar to those reported for inorganic and bio-based cryogels and aerogels (power from 3 to 4) [34–36]. It should be noted that cell morphology and cell shape anisotropy ratio vary with amylopectin concentration and, as a consequence, with material density (see the discussion on the morphology in the section above and Fig. 3). A detailed description of porous amylopectin mechanical properties is not in the scope of this study. What we want to show here is that the values of the compressive modulus in the longitudinal direction at the density around 0.1 g/cm^3 are higher than those of freeze-dried wheat or corn starch (density: 0.12 g/cm^3) [14] and similar to the freeze-dried cellulose II (density: 0.08 ~ 0.10 g/cm^3) [35] or amylopectin reinforced with microfibrillated cellulose (density: 0.09 ~ 0.11 g/cm^3) [7]; however, in our case no reinforcement was used.

3.3 Thermal conductivity

Different porous polymer materials, including bio-based ones, can be used for thermal insulation. In the first approximation, the thermal conductivity λ of a porous material is a sum of the solid λ_{solid}, gas λ_{gas} and radiation λ_{rad} components:

$$\lambda = \lambda_{solid} + \lambda_{gas} + \lambda_{rad} \quad (3)$$

Heat transfer by convection can be neglected when the size of the pores is smaller than about 1 mm, and radiation conductivity is low for optically thick materials at not elevated temperature. Thermal conductivity of the solid phase is power-law dependent on material density, and thus one of the ways to decrease the total thermal conductivity is to decrease material bulk density. The heat transfer through a gaseous phase depends on material porosity ϕ and pore size D:

$$\lambda_g = \frac{\phi \lambda_{g0}}{1+2\beta l/D} \quad (4)$$

where λ_{g0} is the thermal conductivity of the free gas, β is a constant value usually around 1.5 and l is the average free path of the gas molecule (around 70 nm for the air in ambient conditions). For a material of a given porosity, gas thermal conductivity can be decreased by decreasing pore diameter, and below l value λ_g may become lower than λ_{g0} (Knudsen effect). This means that low-density porous materials with pores' dimensions below 70 nm may possess thermal conductivity below that of air (0.025 W/(m·K)). This is the case of some inorganic or organic aerogels including some bio-aerogels based on pectin, starch, nanocellulose or alginate that are intrinsically thermal superinsulating materials [8]. Thermal conductivity can thus be considered as a physical property of a material reflecting not only its thermal, but also morphological properties. For example, by varying the size of the pores by compression, the thermal conductivity of 2,3-dicarboxyl nanocellulose aerogels was decreased from 0.030 to 0.018 W/(m·K) [37].

The thermal conductivity of anisotropic porous starches was measured in longitudinal and transverse directions (Fig. 5). The thermal conductivity in the transverse direction is lower (around 0.04 W/(m·K)) than that in the longitudinal direction (around 0.06 W/(m·K)) (Fig. 5a); a similar trend was reported for freeze-dried nanowood [38,39], bacterial cellulose/polyimide [40] and nanocellulose/graphene oxide [30]. As expected from the morphology of the obtained porous starch materials (Fig. 3 and S3) and eq. 3 and 4, thermal conductivity is low but higher than that of air because of large size of the pores. Interestingly, the conductivity practically does not vary with either material density (Fig. 5a) or retrogradation time (Fig. 5b) within the ranges investigated which can be explained by the simultaneous evolution of cell morphology and density with the increase of starch concentration (Fig. 3).

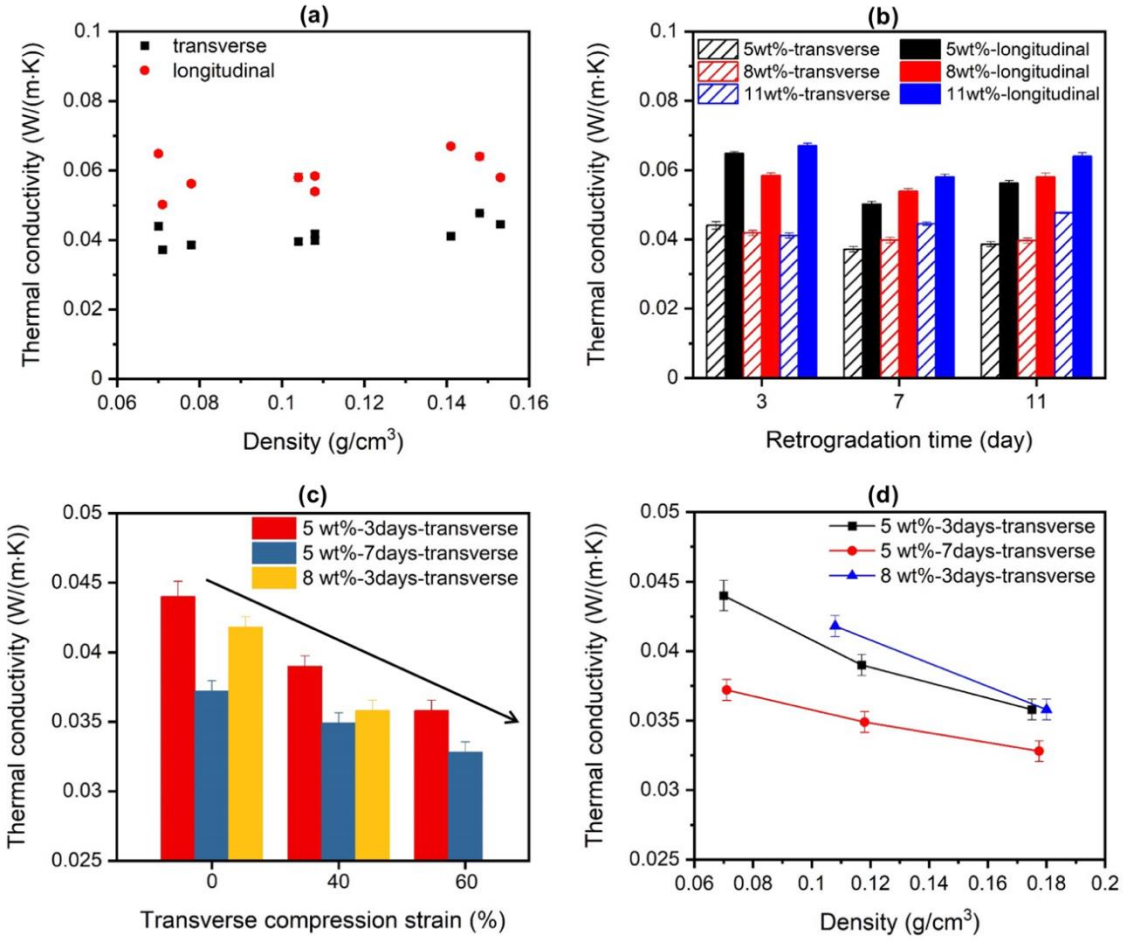

Fig. 5.

Thermal conductivity of waxy maize porous starches: (a) as a function of density (non-compressed), (b) as a function of retrogradation time (non-compressed), (c) as a function of compression strain and (d) as a function of density for compressed samples. Lines are given to guide the eye.

We used the approach applied to aerogels based on nanofibrillated 2,3-dicarboxyl cellulose [37] and evaluated the thermal conductivity of compressed waxy maize porous starches (Fig. 5c,d). The compression strain was varied up to 60% (Fig. 5c). Interestingly, more the material was compressed, lower was the conductivity (Fig. 5c) despite some increase of material density after compression

(Fig. 5d). The result obtained is due to the decrease of pores' size under compression. This phenomenon is reported for porous starch for the first time; it opens the way of tuning thermal conductivity of porous starch materials by a simple mechanical action.

It is worth noting that waxy maize porous starch materials prepared in this work perform well in terms of thermal conductivity in the transverse direction as compared to other porous starch materials, see Table 1. Because of large pores, all freeze-dried starches possess thermal conductivity higher than that of air, as expected. Only some starch aerogels are thermal superinsulating materials thanks to the preservation of mesoporosity when drying with supercritical CO_2 [8,14].

Table 1. Thermal conductivity of porous starch materials made via freeze-drying and supercritical drying.

Starch type	Additional component	Density (g/cm^3)	Thermal conductivity (W/(m·K))	Drying method	Reference
Wheat starch Corn starch	-	0.12 0.12	0.040 0.040	freeze drying	[14]
Potato starch	konjac glucomannan/ wheat straw	0.021-0.054	0.047-0.053	freeze drying	[41]
Amylopectin hydrate (from waxy corn)	sodium montmorillonite	0.0254-0.0288	0.034-0.036 (perpendicular to ice growth direction)	freeze drying	[42]
Starch		0.098	0.041	freeze drying	[43]
	nano fibrillated cellulose	0.013-0.082	0.042-0.054		
Wheat starch Corn starch High amylose corn starch		0.26 0.29 0.15	0.036 0.033 0.024	supercritical drying	[14]
Pea starch	-	0.1	0.021	supercritical drying	[9]

Waxy maize starch	-	0.070-0.153	0.037-0.048 (perpendicular to ice growth direction)	freeze drying	this work
		0.18	0.033 (compressed in the direction perpendicular to ice growth)		

4. Conclusions

Waxy maize porous starch materials with tunable anisotropic morphology, mechanically strong and of low thermal conductivity were made through unidirectional freezing and ice sublimation. No crosslinking or reinforcement was used. Pore structure varied from slit-like to sponge-like adapting to the growth of ice crystals on one hand and controlled by starch concentration on the other hand. Slit-like pores were formed at low starch concentration (5 wt%), the increase of starch concentration led to a larger number of "bridges" between lamellas (8 wt%), and, finally, a uniform spongy matrix without any distinction between lamellas and bridges was at the highest starch concentration (11 wt%). Density varied from 0.07 to 0.15 g/cm^3.

Anisotropic morphology induced anisotropic mechanical and thermal conductivity properties of waxy maize porous starches. Compressive modulus in the direction parallel to the growth of ice crystals (longitudinal direction) is about one order of magnitude higher than the one in the direction perpendicular to the growth of ice crystals (transversal direction). The former varies from around 2.9 to 14.9 MPa and the latter from 0.08 to 0.37 MPa. Toughness varies from few tens to about 100 kJ/m^3. Thermal conductivity of porous starches is low, 0.037 – 0.067 (W/(m·K)) and it is lower in the transverse direction. Further decrease of thermal conductivity was achieved by compressing

the porous starch material in the transverse direction, reaching the values as low as 0.033 (W/(m·K)) when compressed at 60% strain.

Overall, we provide the "recipes" for making fully biobased porous materials with controlled anisotropic morphology and properties that can be used as templates for various applications, from biomedical as scaffolds for cells growth or engineering for sound or thermal insulation or electromagnetic waves absorption.

Acknowledgments

Authors are grateful to Roquette for sponsoring the work and providing starches, to Pierre Ilbizian (PERSEE, MINES Paris) for thermal insulation measurement and to Suzanne Jacomet (CEMEF, MINES Paris) for the help with SEM imaging. We thank Sujie Yu (CEMEF, Mines Paris) for checking porous starches solubility.

CRediT authorship contribution statement

Fangxin Zou.: data curation, formal analysis, methodology, writing- original draft, writing - review & editing; **Jean-Luc Bouvard** and **Christophe Pradille**: mechanical properties measurement, formal analysis, writing - original draft, writing - review & editing; **Tatiana Budtova**: formal analysis, funding acquisition, methodology, project administration, resources, writing - original draft, writing - review & editing.

Declaration of Competing Interest

The authors declare that they have no known competing financial interests or personal relationships that could have appeared to influence the work reported in this paper.

Data availability statement

The raw/processed data required to reproduce these findings cannot be shared at this time as the data also forms part of an ongoing study.

References

[1] T. Budtova, D.A. Aguilera, S. Beluns, L. Berglund, C. Chartier, E. Espinosa, S. Gaidukovs, A. Klimek-kopyra, A. Kmita, D. Lachowicz, F. Liebner, O. Platnieks, A. Rodríguez, L.K.T. Navarro, F. Zou, S.J. Buwalda, Biorefinery approach for aerogels, Polymers. 12 (2020) 1–63. https://doi.org/10.3390/polym12122779.

[2] Q. Zheng, Y. Tian, F. Ye, Y. Zhou, G. Zhao, Fabrication and application of starch-based aerogel: Technical strategies, Trends Food Sci. Technol. 99 (2020) 608–620. https://doi.org/10.1016/j.tifs.2020.03.038.

[3] G.M. Glenn, A. Klamczynski, B. Sen Chiou, W.J. Orts, S.H. Imam, D.F. Wood, Temperature related structural changes in wheat and corn starch granules and their effects on gels and dry foam, Starch/Staerke. 60 (2008) 476–484. https://doi.org/10.1002/star.200800203.

[4] C. Chi, X. Li, Y. Zhang, S. Miao, L. Chen, L. Li, Y. Liang, Understanding the effect of freeze-drying on microstructures of starch hydrogels, Food Hydrocoll. 101 (2020) 105509. https://doi.org/10.1016/j.foodhyd.2019.105509.

[5] B. Zhang, K. Wang, J. Hasjim, E. Li, B.M. Flanagan, M.J. Gidley, S. Dhital, Freeze-drying changes the structure and digestibility of B-polymorphic starches, J. Agric. Food Chem. 62 (2014) 1482–1491. https://doi.org/10.1021/jf405196m.

[6] J.C. Spada, C.P.Z. Noreña, L.D.F. Marczak, I.C. Tessaro, Study on the stability of β-carotene microencapsulated with pinhão (Araucaria angustifolia seeds) starch, Carbohydr. Polym. 89 (2012) 1166–1173. https://doi.org/10.1016/j.carbpol.2012.03.090.

[7] A.J. Svagan, M.A.S.A. Samir, L.A. Berglund, Biomimetic foams of high mechanical performance based on nanostructured cell walls reinforced by native cellulose nanofibrils, Adv. Mater. 20 (2008) 1263–1269. https://doi.org/10.1002/adma.200701215.

[8] F. Zou, T. Budtova, Polysaccharide-based aerogels for thermal insulation and superinsulation: An overview, Carbohydr. Polym. 266 (2021) 118130. https://doi.org/10.1016/j.carbpol.2021.118130.

[9] L. Druel, R. Bardl, W. Vorwerg, T. Budtova, Starch Aerogels: A Member of the Family of Thermal Superinsulating Materials, Biomacromolecules. 18 (2017) 4232–4239. https://doi.org/10.1021/acs.biomac.7b01272.

[10] G. Shao, D.A.H. Hanaor, X. Shen, A. Gurlo, Freeze Casting: From Low-Dimensional Building Blocks to Aligned Porous Structures—A Review of Novel Materials, Methods, and Applications, Adv. Mater. 32 (2020) 1907176. https://doi.org/10.1002/adma.201907176.

[11] V.I. Lozinsky, I.Y. Galaev, F.M. Plieva, I.N. Savina, H. Jungvid, B. Mattiasson, Polymeric cryogels as promising materials of biotechnological interest, Trends Biotechnol. 21 (2003) 445–451. https://doi.org/10.1016/j.tibtech.2003.08.002.

[12] J. Nakamatsu, F.G. Torres, O.P. Troncoso, Y. Min-Lin, A.R. Boccaccini, Processing and characterization of porous structures from chitosan and starch for tissue engineering scaffolds, Biomacromolecules. 7 (2006) 3345–3355. https://doi.org/10.1021/bm0605311.

[13] E.K. Silva, V.M. Azevedo, R.L. Cunha, M.D. Hubinger, M.A.A. Meireles, Ultrasound-assisted encapsulation of annatto seed oil: Whey protein isolate versus modified starch, Food

Hydrocoll. 56 (2016) 71–83. https://doi.org/10.1016/j.foodhyd.2015.12.006.

[14] G.M. Glenn, D.W. Irving, Starch-Based Microcellular Foams, Cereal Chem. 72 (1995) 155–161.

[15] F. Zou, T. Budtova, Tailoring the morphology and properties of starch aerogels and cryogels via starch source and process parameter, Carbohydr. Polym. 255 (2021) 117344. https://doi.org/10.1016/j.carbpol.2020.117344.

[16] V. Baudron, P. Gurikov, I. Smirnova, S. Whitehouse, Porous starch materials via supercritical-and freeze-drying, Gels. 5 (2019) 9–13. https://doi.org/10.3390/gels5010012.

[17] J. Shan, D. Liu, F. Su, M. Li, H. Tian, M. Guo, W. Qiao, J. He, Q. Li, J. Qian, Anisotropic Structure and Properties of Chitin and Chitosan Nanofibril-Supported Starch Foams, ACS Sustain. Chem. Eng. 8 (2020) 17387–17396. https://doi.org/10.1021/acssuschemeng.0c05484.

[18] X. Ni, F. Ke, M. Xiao, K. Wu, Y. Kuang, H. Corke, F. Jiang, The control of ice crystal growth and effect on porous structure of konjac glucomannan-based aerogels, Int. J. Biol. Macromol. 92 (2016) 1130–1135. https://doi.org/10.1016/j.ijbiomac.2016.08.020.

[19] V.I. Lozinsky, Cryostructuring of polymeric systems. 50.† cryogels and cryotropic gel-formation: Terms and definitions, Gels. 4 (2018) 77. https://doi.org/10.3390/gels4030077.

[20] Pierre, A. C. (2011). Aerogels handbook (advances in sol-gel derived materials and technologies). In M. A. Aegerter, N. Leventis, & M. M. Koebel (Eds.), History of aerogels (pp. 3–18). New York Dordrecht Heidelberg London: Springer Science and Business Media.

[21] IUPAC (2014) Compendium of Chemical Terminology, 2nd ed. (the "Gold Book"). Compiled by McNaught AD, Wilkinson A. Blackwell Scientific Publications, Oxford (1997). XML on ‐ line corrected version: http://goldbook.iupac.org (2006) created by M.

Nic, J. Jirat, B. Kosata; updates compiled by A. Jenkins. ISBN 0-9678550-9-8. https://doi.org/10.1351/goldbook. Last update 2014-02-24; version: 2.3.3.

[22] K. Ganesan, T. Budtova, L. Ratke, P. Gurikov, V. Baudron, I. Preibisch, P. Niemeyer, I. Smirnova, B. Milow, Review on the production of polysaccharide aerogel particles, Materials. 11 (2018) 1–37. https://doi.org/10.3390/ma11112144.

[23] C.A. García-González, I. Smirnova, Use of supercritical fluid technology for the production of tailor-made aerogel particles for delivery systems, J. Supercrit. Fluids. 79 (2013) 152–158. https://doi.org/10.1016/j.supflu.2013.03.001.

[24] S. Groult, T. Budtova, Thermal conductivity/structure correlations in thermal super-insulating pectin aerogels, Carbohydr. Polym. 196 (2018) 73–81. https://doi.org/10.1016/j.carbpol.2018.05.026.

[25] C. Rudaz, R. Courson, L. Bonnet, S. Calas-Etienne, H. Sallée, T. Budtova, Aeropectin: Fully biomass-based mechanically strong and thermal superinsulating aerogel, Biomacromolecules. 15 (2014) 2188–2195. https://doi.org/10.1021/bm500345u.

[26] L. Druel, P. Niemeyer, B. Milow, T. Budtova, Rheology of cellulose-[DBNH][CO2Et] solutions and shaping into aerogel beads, Green Chem. 20 (2018) 3993–4002. https://doi.org/10.1039/c8gc01189c.

[27] B. Chen, Q. Zheng, J. Zhu, J. Li, Z. Cai, L. Chen, S. Gong, Mechanically strong fully biobased anisotropic cellulose aerogels, RSC Adv. 6 (2016) 96518–96526. https://doi.org/10.1039/c6ra19280g.

[28] S. Christoph, A. Hamraoui, E. Bonnin, C. Garnier, T. Coradin, F.M. Fernandes, Ice-templating beet-root pectin foams: Controlling texture, mechanics and capillary properties, Chem. Eng. J. 350 (2018) 20–28. https://doi.org/10.1016/j.cej.2018.05.160.

[29] H.K. Chang, C.W. Huang, C.C. Chiu, H.J. Wang, P.Y. Chen, Fabrication of anisotropic poly(vinyl alcohol) scaffolds with controllable mechanical properties and structural recoverability under compression via a freeze-casting technique, Macromolecules. 53 (2020) 8809–8818. https://doi.org/10.1021/acs.macromol.0c01608.

[30] B. Wicklein, A. Kocjan, G. Salazar-Alvarez, F. Carosio, G. Camino, M. Antonietti, L. Bergström, Thermally insulating and fire-retardant lightweight anisotropic foams based on nanocellulose and graphene oxide, Nat. Nanotechnol. 10 (2015) 277–283. https://doi.org/10.1038/nnano.2014.248.

[31] M. Yang, Y. Yuan, Y. Li, X. Sun, S. Wang, L. Liang, Y. Ning, J. Li, W. Yin, Y. Li, Anisotropic Electromagnetic Absorption of Aligned Ti3C2T xMXene/Gelatin Nanocomposite Aerogels, ACS Appl. Mater. Interfaces. 12 (2020) 33128–33138. https://doi.org/10.1021/acsami.0c09726.

[32] L.J. Gibson, M.F. Ashby, Cellular Solids: Structure and Properties, Cambridge Univ. Press. (1997).

[33] S. Faraji, K. L. Stano, O. Yildiz, A. Li, Y. Zhu, P.D. Bradford, Ultralight anisotropic foams from layered aligned carbon nanotube sheets, Nanoscale. 7 (2015) 17038–17047. https://doi.org/10.1039/c5nr03899e.

[34] G.W. Scherer, D.M. Smith, X. Qiu, J.M. Anderson, Compression of aerogels, J. Non. Cryst. Solids. 186 (1995) 316–320. https://doi.org/10.1016/0022-3093(95)00074-7.

[35] N. Buchtová, C. Pradille, J.L. Bouvard, T. Budtova, Mechanical properties of cellulose aerogels and cryogels, Soft Matter. 15 (2019) 7901–7908. https://doi.org/10.1039/c9sm01028a.

[36] F. Martoïa, T. Cochereau, P.J.J. Dumont, L. Orgéas, M. Terrien, M.N. Belgacem, Cellulose

nanofibril foams: Links between ice-templating conditions, microstructures and mechanical properties, Mater. Des. 104 (2016) 376–391. https://doi.org/10.1016/j.matdes.2016.04.088.

[37] S.F. Plappert, J.M. Nedelec, H. Rennhofer, H.C. Lichtenegger, F.W. Liebner, Strain Hardening and Pore Size Harmonization by Uniaxial Densification: A Facile Approach toward Superinsulating Aerogels from Nematic Nanofibrillated 2,3-Dicarboxyl Cellulose, Chem. Mater. 29 (2017) 6630–6641. https://doi.org/10.1021/acs.chemmater.7b00787.

[38] T. Li, J. Song, X. Zhao, Z. Yang, G. Pastel, S. Xu, C. Jia, J. Dai, C. Dai, A. Gong, F. Jiang, Y. Yao, T. Fan, B. Yang, L. Wågberg, R. Yang, L. Hu, Anisotropic, lightweight, strong, and super thermally insulating nanowood with naturally aligned nanocellulose, Sci. Adv. 4 (2018) 1–10. https://doi.org/10.1126/sciadv.aar3724.

[39] J. Song, C. Chen, Z. Yang, Y. Kuang, T. Li, Y. Li, H. Huang, I. Kierzewski, B. Liu, S. He, T. Gao, S.U. Yuruker, A. Gong, B. Yang, L. Hu, Highly Compressible, Anisotropic Aerogel with Aligned Cellulose Nanofibers, ACS Nano. 12 (2018) 140–147. https://doi.org/10.1021/acsnano.7b04246.

[40] X. Zhang, X. Zhao, T. Xue, F. Yang, W. Fan, T. Liu, Bidirectional anisotropic polyimide/bacterial cellulose aerogels by freeze-drying for super-thermal insulation, Chem. Eng. J. 385 (2020) 123963. https://doi.org/10.1016/j.cej.2019.123963.

[41] Y. Wang, K. Wu, M. Xiao, S.B. Riffat, Y. Su, F. Jiang, Thermal conductivity, structure and mechanical properties of konjac glucomannan/starch based aerogel strengthened by wheat straw, Carbohydr. Polym. 197 (2018) 284–291. https://doi.org/10.1016/j.carbpol.2018.06.009.

[42] D.D. Ye, T. Wang, W. Liao, H. Wang, H.B. Zhao, Y.T. Wang, S. Xu, Y.Z. Wang, Ultrahigh-Temperature Insulating and Fire-Resistant Aerogels from Cationic Amylopectin and Clay

via a Facile Route, ACS Sustain. Chem. Eng. 7 (2019) 11582–11592. https://doi.org/10.1021/acssuschemeng.9b01487.

[43] N. Yildirim, S.M. Shaler, D.J. Gardner, R. Rice, D.W. Bousfield, Cellulose nanofibril (CNF) reinforced starch insulating foams, Cellulose. 21 (2014) 4337–4347. https://doi.org/10.1007/s10570-014-0450-9.

Supporting Information

Ice-templated Additive-free Porous Starches with Tuned Morphology and Properties

Fangxin Zou[a], Jean-Luc Bouvard[a], Christophe Pradille[b], Tatiana Budtova[a]*

[a] MINES Paris, PSL Research University, Center for Materials Forming (CEMEF), UMR CNRS 7635, CS 10207, 06904 Sophia Antipolis, France

[b] Mat Xper, 19 Traverse du Barri, 06560, Sophia Antipolis, France

* Corresponding author: Tatiana Budtova, e-mail address: tatiana.budtova@minesparis.psl.eu

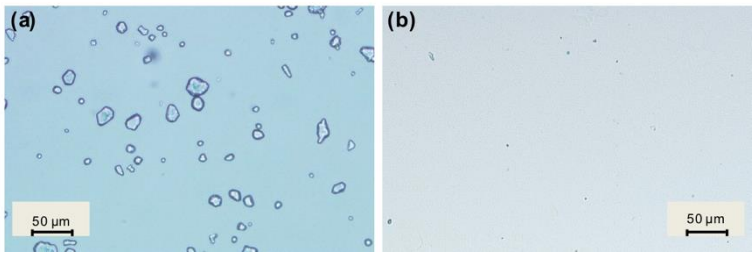

Fig. S1.

Optical microscope images of waxy maize starch before (a) and after heating at 95 °C for 3 h.

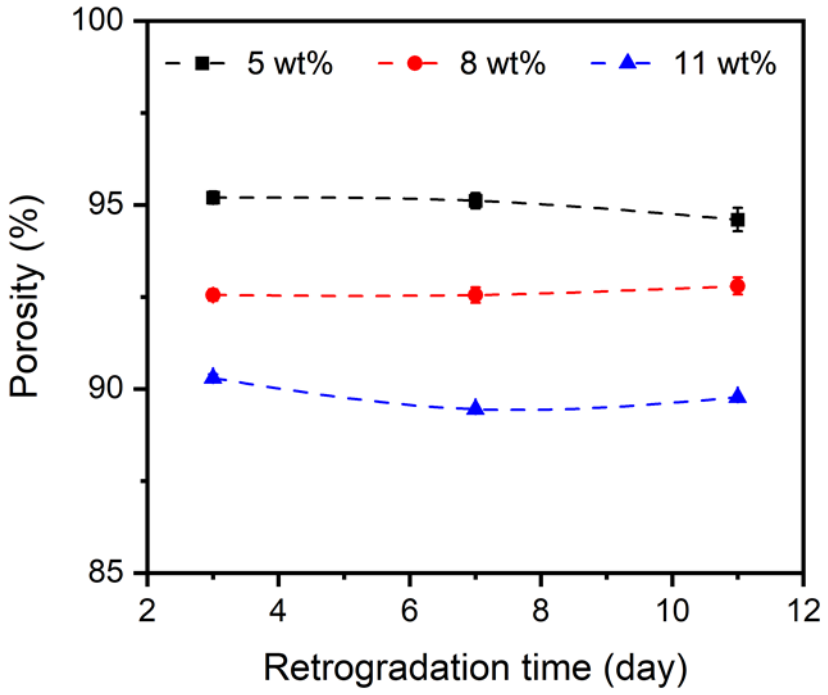

Fig. S2.

Porosity of waxy maize porous starch materials from different starch concentrations as a function of retrogradation time. If the errors are not seen, they are smaller or equal to the symbol. Lines are given to guide the eye.

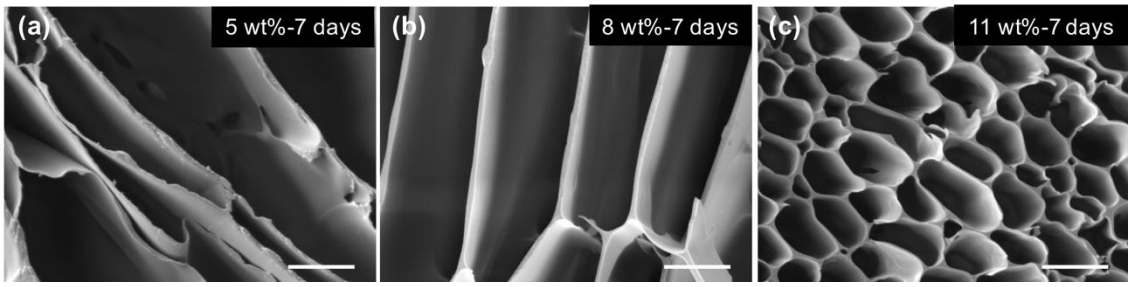

Fig. S3.

SEM images of the cross-section of waxy maize porous starches made from starch concentrations of 5 wt%, 8 wt% and 11 wt%, all after 7 days retrogradation. Scale bars are 10 µm.

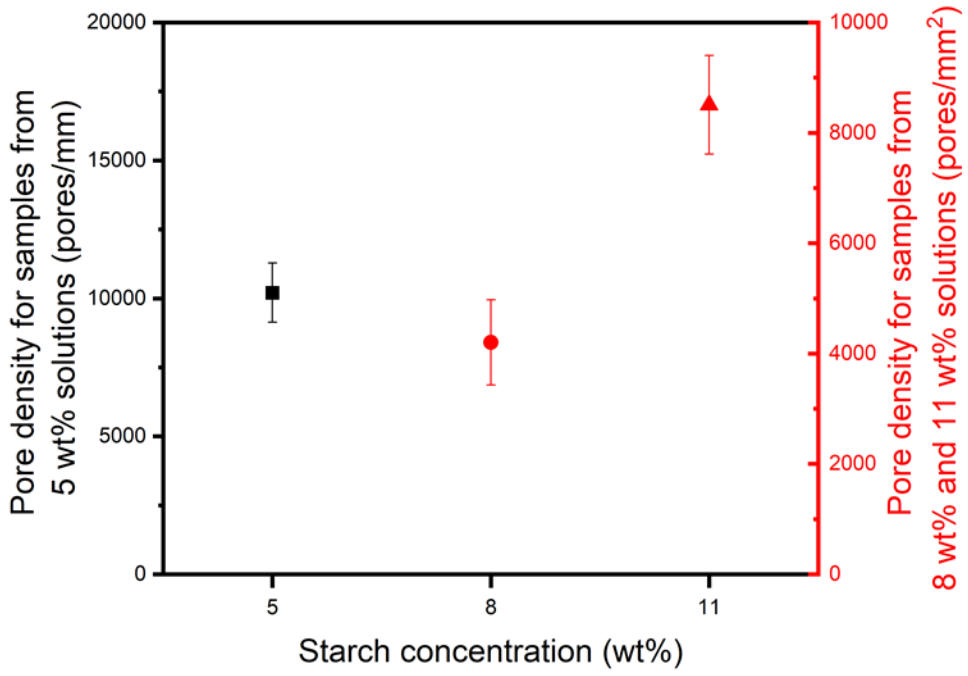

Fig. S4.

Pore density of waxy maize porous starches made from starch solutions of concentrations 5 wt% (in black), and 8 wt% and 11 wt% (in red), all after 3 days retrogradation.